JOURNAL OF MATERIALS SCIENCE 27 (1992) 5181–5191

Elevated-temperature crack growth in polycrystalline alumina under static and cyclic loads

L. EWART*, S. SURESH
Division of Engineering, Brown University, Providence, RI 02912, USA

An experimental investigation has been conducted to study the crack growth characteristics of a 90% pure aluminium oxide in 1050 °C air under static and cyclic loads. It is shown that the application of both sustained and fluctuating tensile loads to the ceramic, tested in a pre-cracked four-point bend specimen configuration, results in appreciable subcritical crack growth. The crack velocities under cyclic loading conditions are up to two orders of magnitude slower than those measured in static loading under the same maximum stress intensity factor. Cyclic crack growth rates are markedly affected by the loading frequency, with a decrease in test frequency causing an increase in the rate of crack advance. Detailed optical and electron microscopy observations have been made in an attempt to study the mechanisms of stable crack growth and the mechanistic differences between static fatigue fracture. Under both static and cyclic loads, the predominant mode of fracture is intergranular separation. The presence of a glass phase along the grain boundaries appears to have a strong effect on the mechanisms of crack growth. Apparent differences in the crack velocities between static and cyclic fatigue in alumina arise from crack-wake contact effects as well as from the rate-sensitivity of deformation of the glass phase. Our results also indicate that the cyclic fatigue crack growth rates cannot be predicted solely on the basis of sustained load fracture data. While stable crack growth occurs in the 90% pure alumina over a range of stress intensity factor spanning 1.5 to 5 MPa $m^{1/2}$, such subcritical fracture is essentially suppressed in a 99.9% pure alumina, ostensibly due to the paucity of a critical amount of glass phase. Both static and cyclic fracture characteristics of the 90% pure alumina are qualitatively similar to those found in an Al_2O_3–SiC composite where *in situ* formation of glass phases, due to the oxidation of SiC in high-temperature air, is known to be an important factor in the fracture process.

1. Introduction

The increasing demand for lightweight materials with good high-temperature properties and resistance to corrosion and wear has led to a growing interest in advanced ceramics for a wide range of structural applications. Although such potential applications inevitably involve exposure of the ceramic materials to high temperatures and cyclic loading conditions in service, there is a serious lack of understanding of the cyclic fatigue characteristics of ceramics at both ambient and elevated temperatures. This paucity of research effort can be traced to several factors. First, traditional interpretations of cyclic deformation and fracture in metallic materials have centred around the existence of cyclic slip (i.e. to-and-fro dislocation motion). The absence of appreciable dislocation plasticity in ceramic materials is generally considered the reason for the (presumed) absence of a cyclic fatigue effect. Second, the limited amount of experimental information available in the literature on monolithic ceramics has given rise to conflicting conclusions on the existence of a mechanical fatigue effect. For example, some of the work has shown that any stable crack growth occurring in alumina is a consequence of stress corrosion cracking (static fatigue) and that it is not ascribable to any true fatigue effects (e.g. [1, 2]). Some other investigations (e.g. [3–8]) have merely provided stress–life data indicating differences between static and cyclic behaviour without establishing the underlying mechanistic differences. There is also experimental evidence (e.g. [9–11]) suggesting that cyclic fatigue effects take place in ceramics only under certain combinations of test temperature and loading variables. However, in recent years there has been a large body of emerging information which reveals that true cyclic fatigue effects can take place in alumina (e.g. [12–22]). Furthermore, direct evidence of crack growth, attributable solely to fluctuating loads, has also been

* *Present address*: U. S. Army Materials Technology Laboratory, Watertown, MA 02172, USA.

0022–2461

obtained for polycrystalline alumina subjected to cyclic loads at room temperature [16–21].

While the majority of the above studies have centred around exploring room-temperature cyclic fatigue effects in alumina, there is a more serious lack of effort in elucidating the high-temperature cyclic fatigue characteristics of ceramics. This situation is further compounded by the inferences of a few studies on the basis of limited experimental data that the crack growth rates in ceramic materials under cyclic loads can be predicted on the basis of the crack velocities obtained from static load creep fracture (e.g. [1, 23]). More recent work [20, 24–26] covering a broader range of test variables and loading conditions has shown that there can be significant differences in the mechanisms of crack advance and crack-wake contact between static and cyclic fracture in ceramic materials at elevated temperatures. Detailed transmission electron microscopy of crack-tip damage in an Al_2O_3–SiC whisker composite has revealed intrinsic differences in the very mechanisms of damage induced by static and cyclic loads [24]. These studies [20, 24–26] reveal that the crack velocities under cyclic loads can be substantially slower than those found under static loads. Furthermore, cyclic stress–life data obtained in the temperature range 1000–1200 °C for Al_2O_3 and Si_3N_4 show that the lifetime under cyclic loads is longer than that under static loads when the static stress is equal to the maximum cyclic stress [27, 28].

The objective of the present work was to investigate the elevated-temperature cyclic fatigue crack growth characteristics of polycrystalline alumina ceramics. The crack velocities observed under cyclic loads are compared with those seen under static loads, and the mechanisms of static fatigue and cyclic fatigue at elevated temperatures are examined in detail. Particular attention is devoted to investigating the possible role of grain boundary amorphous films (introduced during the processing of the material) in influencing static and cyclic fatigue. Experimental results are also obtained on the effects of cyclic frequency on fatigue crack propagation rates. The fatigue behaviour of the monolithic alumina is also compared with that of an Al_2O_3–SiC composite in an attempt to extract some mechanistic information on the effects of viscous amorphous films on stable crack growth. It is hoped that the results of this study will lead to a better understanding of the effects of cyclic loads on stable fracture in ceramics at high temperatures.

2. Experimental procedure

The ceramic materials investigated consisted of two grades of polycrystalline aluminium oxide, Al_2O_3, commercially available as AD 90 and AD 999 from Coors Porcelain Co., Boulder, Colorado. AD 90 and AD 999 are 90% and 99.9% pure aluminium oxide, respectively. The main impurities in the AD 90, added as sintering aids, are silica, magnesia and calcia with trace amounts of iron oxide, sodium oxide and potassium oxide. Such impurities are expected to be present to a significantly smaller extent in the AD 999 alumina. Fig. 1 shows an as-received microstructure of AD 90 alumina where the transmission electron micrographs reveal the crystalline grains surrounded by an amorphous phase.

The material properties of the AD 90 alumina are as follows: tensile strength (25 °C) of 221 MPa, tensile strength (1000 °C) of 103 MPa, compressive strength (25 °C) of 2482 MPa, compressive strength (1000 °C) of 517 MPa, flexural strength (25 °C) of 338 MPa, Young's modulus of 276 GPa, range of grain sizes of 2–10 μm with an average grain size of 4 μm. For the AD 999 alumina, the mechanical properties are: tensile strength (25 °C) of 310 MPa, tensile strength (1000 °C) of 221 MPa, compressive strength (25 °C) of 3792 MPa, compressive strength (1000 °C) of 1930 MPa, flexural strength (25 °C) of 552 MPa, flexural strength (1000 °C) of 414 MPa, Young's modulus of 386 GPa, range of grain sizes 1–6 μm with an average grain size of 3 μm.

All testing was done in a servohydraulic testing machine on single-edge notched specimens measuring 50.8 mm × 10 mm × 9 mm. Notches (of root radius ~ 150 μm) were introduced with a resin-bonded diamond blade to a depth such that the notch depth to specimen width ratio was 0.4. The side surfaces of the specimens were polished down to a roughness of better than 6 μm. The specimens were precracked at

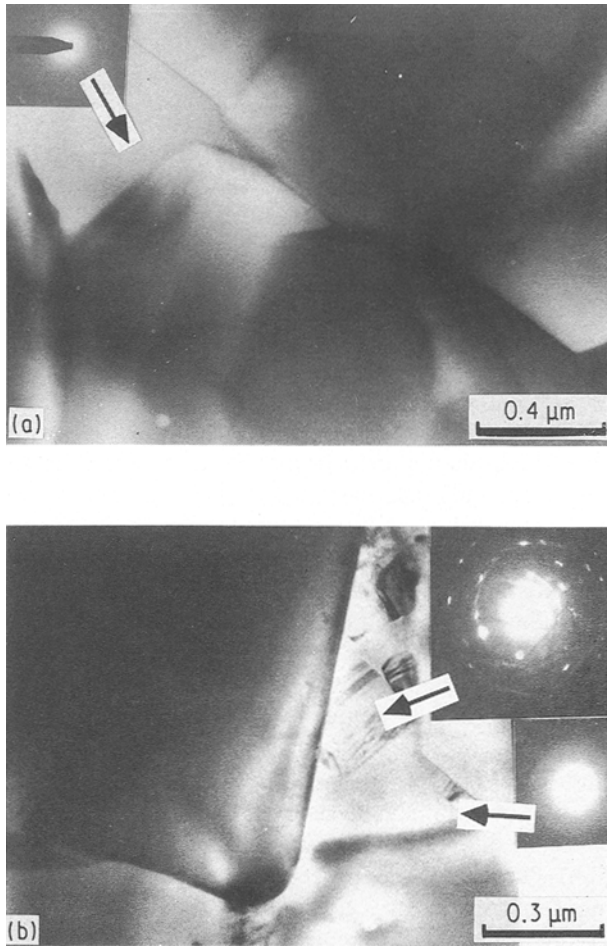

Figure 1 (a, b) Transmission electron micrographs of the as-received microstructure of AD 90 alumina. The accompanying diffraction patterns in (b) reveal crystalline regions inside the glass pockets

room temperature in uniaxial cyclic compression using a procedure detailed elsewhere [16–19]. The length of the self-arresting, through-thickness precrack was typically 0.4 mm. High-temperature tests were performed in a four-point bend fixture having an inner span of 20 mm and an outer span of 40 mm. The notch and precrack were placed in tension in the four-point bend flexural loading arrangement. For high-temperature mechanical testing a programmable furnace was mounted on a servohydraulic testing machine. The furnace was programmed to heat up to 1050°C at 13°C min^{-1} and to cool down to room temperature at 21°C min^{-1}. Specimens were not loaded during heat-up or cool-down. They were allowed to equilibrate at test temperature for at least 5 min before the loads were imposed and the tests were begun. Cyclic fatigue specimens were loaded to the minimum stress intensity factor, K_{min}, and immediately cycled between this minimum load and the predetermined maximum load. The number of cycles a specimen experienced varied depending on the expected growth rates. Tests were run at frequencies, ν_c, of 0.13 and 2 Hz (sinusoidal waveform) and a load ratio of 0.15. (The load ratio, R, is defined as the ratio of the minimum load to the maximum load of the fatigue cycle.) Static crack growth experiments were also conducted in the same elevated-temperature environment, using the same specimen geometry and pre-cracking techniques, in order to compare cyclic fatigue and static fatigue behaviour. All the experiments were conducted at least twice and the results presented in this paper represent information derived from duplicate experiments.

In the high-temperature environment, the specimens were initially subject to a small tensile (static or cyclic) load, depending on the experiment, with the initial stress intensity factor (or stress intensity range for the cyclic fatigue test) typically smaller than 0.5 MPa $m^{1/2}$. If no crack growth occurred (at rates in excess of 10^{-10} m $cycle^{-1}$), the stress intensity factor was incremented by approximately 10%. This procedure was repeated until crack growth was detected; following the onset of crack growth from the tip of the precrack, static and cyclic fracture experiments were allowed to proceed at constant far-field loads. After the static test or load cycling, the load was removed; the furnace was slowly cooled down to room temperature and the specimen was removed for monitoring crack growth.

Crack growth was monitored by periodically interrupting the tests (using the procedure described above) and making replicas of both side surfaces of the specimen using an acetate replica film. Replica film is known to shrink slightly and give smaller than expected values if measurements are taken over large areas. To avoid this error, the change in crack length between tests was measured instead of the total crack length. Measurements were taken in an optical microscope containing a calibrated eyepiece.

Mechanisms of static and cyclic fatigue crack growth were investigated in detail by recourse to scanning and transmission electron microscopy (SEM and TEM, respectively). TEM specimens were made by gluing together the fractured halves of the test specimens. Thin slices were made perpendicular to the plane of the crack and to the crack front. Circular discs, about 3 mm in diameter, were drilled out from appropriate positions along the crack profile. This was followed by dimpling, ion milling and carbon coating, prior to making observations in a Philips 420 scanning transmission electron microscope.

3. Results

3.1. Crack growth behaviour in static and cyclic tension

Fig. 2 shows the variation of fatigue crack growth per load cycle, da/dN, as a function of the nominal value of stress intensity factor range, ΔK, for the AD 90 alumina subjected to fatigue loads at $R = 0.15$ at test frequencies of 0.13 and 2.0 Hz in 1050°C air. This figure shows that subcritical crack growth occurs over the ΔK range 1.5–5 MPa $m^{1/2}$. Despite the normal experimental scatter associated with batch variability, good reproducibility was found between duplicate experiments. Since the size scale of the inelastic damage zone ahead of the advancing fatigue crack is small compared to the dimensions of the specimen (including the crack size and the size of the uncracked ligament) for the conditions of the present experiments, the stress intensity factor range was found to characterize the growth rates. Furthermore, despite the experimental scatter in the intermediate (Paris) regime of fatigue crack growth, a linear dependence exists between log (da/dN) and log (ΔK) such that $da/dN = C(\Delta K)^m$. The constants C and m are listed in Table I for the AD 90 alumina. At any given ΔK value, a crack propagating under a cyclic frequency of 2 Hz

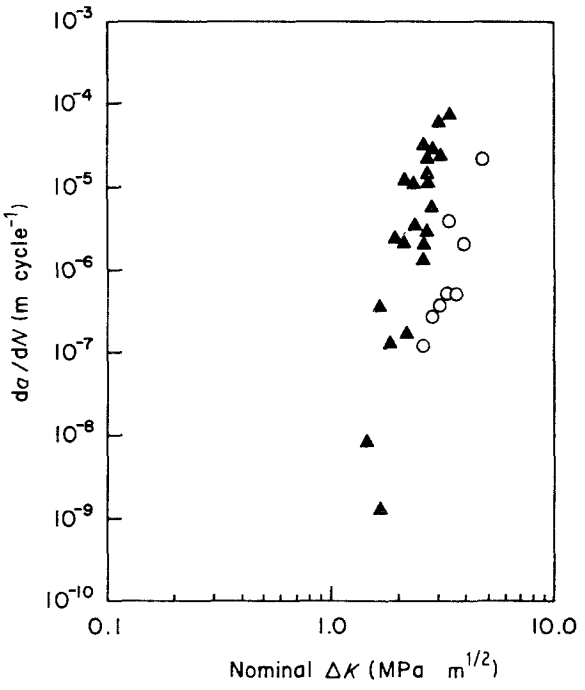

Figure 2 Variation of fatigue crack growth rate, da/dN, as a function of the nominal stress intensity factor range, ΔK, for AD 90 alumina cyclically loaded in 1050°C air at $R = 0.15$ and (▲)ν_c = 0.13 Hz and (○)ν_c = 2 Hz.

TABLE I Experimentally determined constants in the equation for cyclic fatigue crack rate growth, $da/dN = C(\Delta K)^m$, or static crack growth rate, $da/dt = A(K_I)^n$ of AD 90 alumina at 1050°C

Test conditions	C (m cycle^{-1} MPa^{-m})	m	A (m cycle^{-1} MPa^{-m})	n	ΔK or K_I (MPa m$^{1/2}$)
Cyclic; $R = 0.15$, $\nu_c = 0.13$ Hz	2.8×10^{-10}	10	–	–	1.0–3.0
Cyclic; $R = 0.15$, $\nu_c = 2$ Hz	6.3×10^{-11}	8	–	–	2.0–3.5
Static	–	–	1.0×10^{-7}	5	1.5–3.5

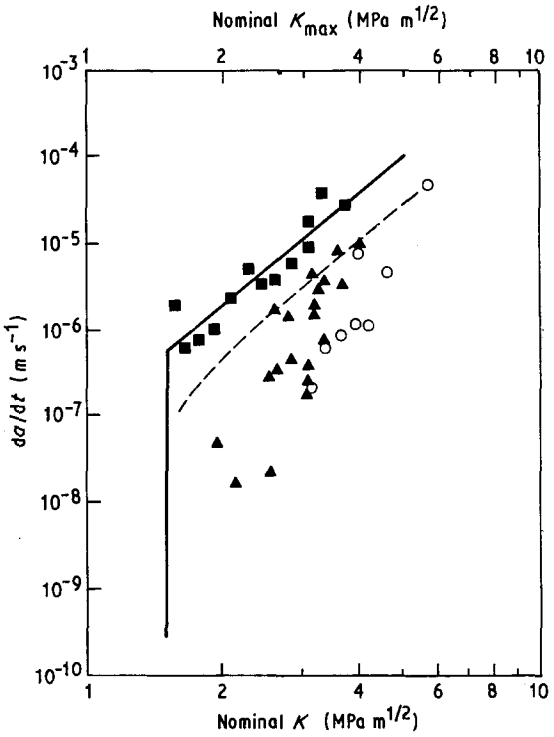

Figure 3 Experimentally measured crack velocity, da/dt, as a function of the stress intensity factor, K_I, for static load fracture of AD 90 alumina in 1050°C air. Also shown are experimentally measured crack velocities, $da/da = \nu_c(da/dN)$, as a function of $K_{max} = \Delta K/(1 - R)$ for cyclic load fracture in 1050°C air at $R = 0.15$ and $\nu_c = (\blacktriangle)0.13$ Hz and (○)2 Hz. the dashed line (– – –) indicates the prediction of cyclic crack growth rates on the basis of static fracture data using Equation 1. See text for details.

shows slower growth rates, by more than an order of magnitude, than under a cyclic frequency of 0.13 Hz.

Fig. 3 shows the crack velocities, da/dt, for the fatigue tests (taken from Fig. 2) as a function of the maximum stress intensity factor values, K_{max}, during the stress cycle. Note that $da/dt = (da/dN)\nu_c$ and that $K_{max} = \Delta K/(1 - R)$. Also indicated in Fig. 3 are the crack velocities for sustained load fracture plotted as a function of the stress intensity factor, K_I. At the same values of K_I and K_{max}, the rate of crack growth under sustained loads is significantly faster than that seen under cyclic loads. This effect is particularly more pronounced at lower stress intensity factor values and higher values of cyclic frequency. The quasi-static crack velocity can be characterized by the expression $da/dt = B(K_I)^n$ where B and n are material constants which are listed in Table I.

Earlier studies (e.g. [1, 23]) of high-temperature fracture in ceramic materials indicated that crack growth under cyclic loading conditions could be predicted on the basis of static crack growth data. Such an approach is an outcome of the assumption that any apparent cyclic fatigue effect is merely a manifestation of static creep behaviour under varying loads. If this assumption were to be true, one possible means of deriving cyclic crack growth rates entails integrating the appropriate static growth rates over one cycle such that

$$\left(\frac{da}{dt}\right)_{cyclic} = \frac{1}{\tau}\int_0^{\tau}\left(\frac{da}{dt}K_I\right)_{static} dt \qquad (1)$$

where the static crack velocity is an experimentally determined function of the stress intensity factor, K_I (i.e. the solid curve in Fig. 3) and $\tau = 1/\nu_c$. The crack growth rates for cyclic loads, predicted on the basis of static fatigue data, are plotted in Fig. 3 (dashed line). For the present set of results obtained for alumina, the results of Fig. 3 clearly indicate that it is not feasible to accurately predict the cyclic fatigue crack velocities solely on the basis of static fatigue data.

A significant result of earlier work [24] on stable crack growth at elevated temperatures in Al_2O_3–SiC composites is that grain boundary glass films, either pre-existing or forming *in situ* in the high-temperature test environment, play an important role in influencing the crack velocities (see later discussions for further details). To explore the implications of this result for polycrystalline alumina, the results of high-temperature crack growth in AD 90 (90% pure) alumina were compared with those obtained from the same experiments conducted on AD 999 (99.9% pure with a significantly smaller extent of pre-existing amorphous phase along grain boundaries). Fig. 4 shows a comparison of the crack velocity versus K_I (or K_{max}) plots for AD 90 and AD 999 alumina in 1050°C air under cyclic ($R = 0.15$ and $\nu_c = 0.13$ Hz) and static loading. While a substantial amount of stable crack growth occurs (over distances of more than 1 mm for the present tests) in the AD 90 alumina over a ΔK range 1.5–5 MPa m$^{1/2}$ under both static and cyclic loads, the flexural tests on the fine-grained AD 999 alumina do not reveal any detectable subcritical fracture (above a growth rate of 10^{-10} m cycle^{-1}) in both static and cyclic fatigue. For this latter material, only catastrophic fast fracture occurs over the K_I or K_{max} range 3.2–4.2 MPa m$^{1/2}$. This scatter band over which final failure takes place is denoted by the two solid lines in Fig. 4. As will be shown in section 4, this trend is also consistent with the results obtained in other studies on Al_2O_3–SiC composites and on low-cycle fatigue tests in alumina.

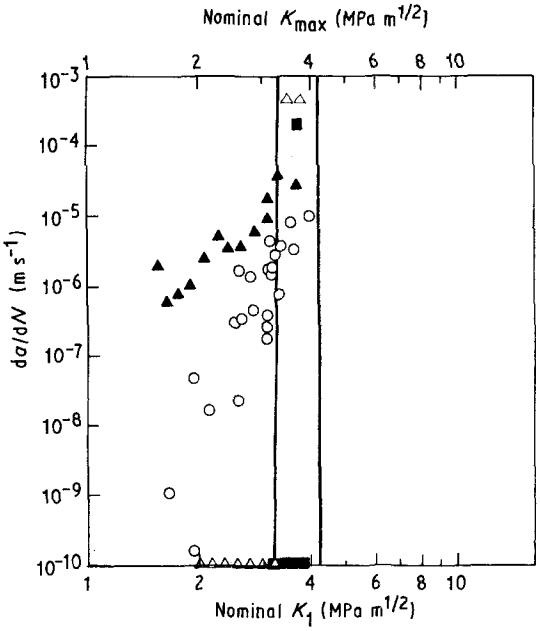

Figure 4 Crack velocity, da/dt, plotted against K_I or K_{max} for (○, ▲) AD 90 and (△, ■) AD 999 alumina under (○, △) cyclic loading ($R = 0.15$ and $\nu_c = 0.13$ Hz) and (▲, ■) static loading in 1050°C air.

3.2. Micromechanisms of subcritical crack growth

Detailed observations of the microscopic mechanisms of crack growth were made in the scanning and transmission electron microscope for test specimens subjected to static and cyclic loads in the elevated-temperature environment. Crack growth in both static and cyclic tension occurs by a predominantly intergranular mode of separation. However, some noticeable differences also exist between the two cases with regard to the manner in which crack faces contact.

A typical crack profile observed on the side surface of a cyclic fatigue specimen of alumina is provided in Fig. 5a. Although this figure specifically shows a crack profile of a specimen tested at $\nu_c = 0.13$ Hz and $R = 0.15$, this profile is typical of all the fatigue cracks. The fatigue crack initiates from a precrack and propagates in a direction generally parallel to the plane of the notch. However, the crack path is microscopically very tortuous. Crack branching is seen ahead of the crack tip as well as along the crack wake.

Fig. 5b–d is a series of micrographs illustrating the microscopic roughness of the crack path and the occurrence of closure (specifically, roughness-induced crack closure [29]) arising from the frictional sliding and contact between the asperities of the mating crack surfaces. While the intergranular mode of fracture evident in Fig. 5 is common to both static and cyclic fatigue in alumina, the conditions of crack wake contact appear to be different. The following observations deal with these issues.

(i) Repeatedly unloading from and reloading to a peak tensile stress in cyclic fatigue causes premature contact (even at a far-field tensile stress) among the fracture surface asperities, as shown for example in Fig. 5b. It is known from the fatigue of metals that

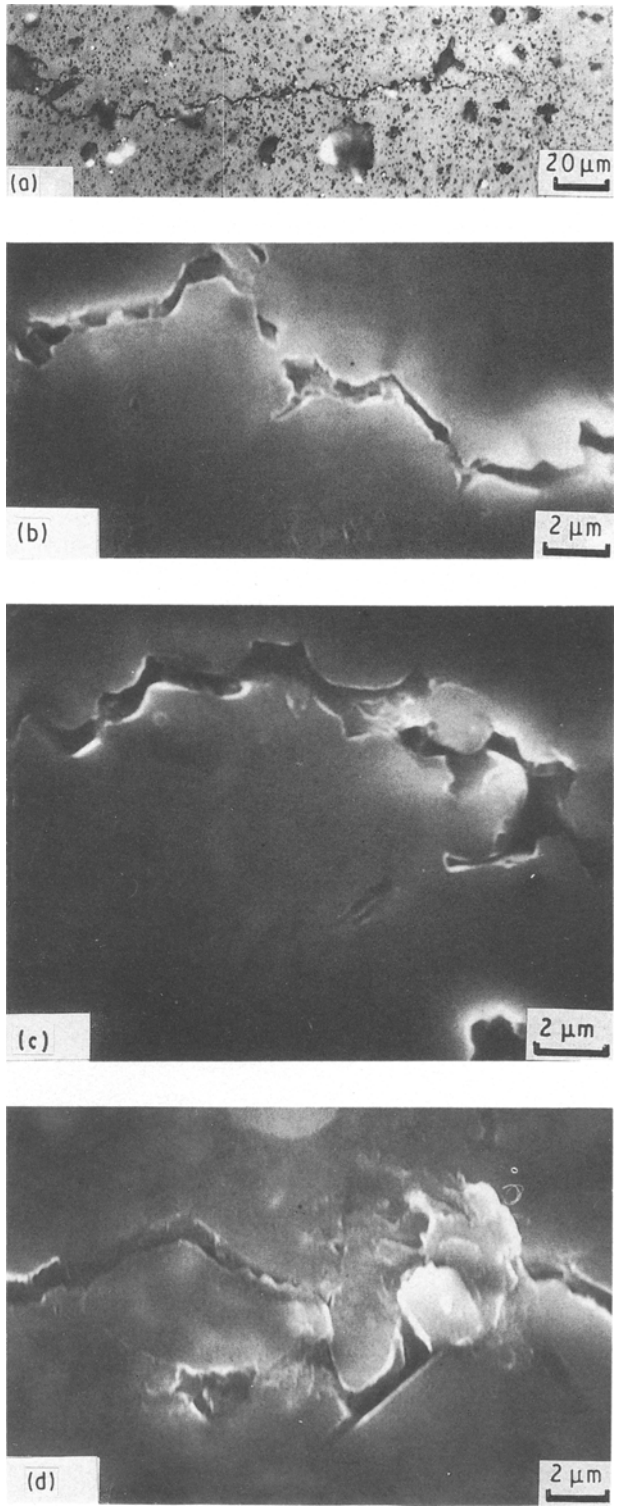

Figure 5 Characteristics of cyclic fatigue cracks in AD 90 alumina. (a) Typical profile of the fatigue crack. (b) Roughness-induced crack closure. (c, d) Debris particles and glass phase being squeezed out of the crack by the pumping action of the crack walls under cyclic loading.

sliding (mode II) displacements between crack faces can occur even for nominally pure mode I fatigue loading as a consequence of a microscopically tortuous crack path (which promotes locally mixed-mode loading conditions) and kinematically irreversible microscopic deformation at the crack tip. Similar trends are also seen during the high-temperature cyclic fracture of polycrystalline alumina. From the

micrographs of crack profiles, the extent of this closure appears to be less pronounced under static loading than under cyclic loading.

(ii) Repeated loading and unloading, in conjunction with crack-face asperity contact, creates debris particles of the ceramic between the crack faces. Clear evidence of this process is found in Fig. 5c and d. The debris particles may further reduce the effective driving force responsible for crack growth. (Experimental results [16, 17] reveal that the presence of debris particles within cracks in alumina retards crack advance under cyclic compression loading at room temperature.) In the case of static fatigue in alumina, the formation of debris particles is substantially less pronounced. Fig. 6 shows a microscopically tortuous crack path in AD 90 alumina subjected to sustained load fracture in the 1050°C air environment. Note the absence of debris particles within the crack, such as those seen in Fig. 5.

(iii) As noted earlier, the AD 90 alumina contains 10% impurities which are retained, predominantly as amorphous films along grain facets, after processing of the material. In the elevated-temperature environment, the amorphous phase undergoes viscous creep. Fig. 7a shows a typical intergranular fracture process during static fatigue of AD 90 alumina at 1050°C. A higher-magnification view of the grain boundary region reveals ligaments of amorphous films bridging the faces of the crack (Fig. 7b). Similar amorphous film ligaments were also seen under cyclic loading conditions. Fig. 8 is a series of scanning electron micrographs of the cyclic fatigue fracture surfaces of AD 90 alumina showing (a) predominantly intergranular fracture (Fig. 8a), (b) grain facets covered with an amorphous phase (Fig. 8b) and (c) an occasional occurence of transgranular cleavage (Fig. 8c). Although the static load failure surfaces exhibited features similar to those seen in Fig. 8, some possible differences between the effects of glass phase in static and cyclic fatigue are evident. This viscous flow and deformation of the amorphous intergranular phase is highly sensitive to the loading rate and test frequency. Consequently, fracture along grain boundary facets populated with the glassy phase would be expected to be strongly affected by whether the loading is static or cyclic and by the frequency of cyclic loading. Furthermore, under cyclic loading conditions, the amorphous film can be "squeezed out" of the crack (similar to Fig. 5d) thereby reducing the bridging of crack faces by the glassy ligaments.

In addition to the above mechanistic processes, both static and cyclic fatigue loading at elevated temperatures resulted in the formation of zones of distributed microcracking along grain boundaries. Fig. 9a shows a transmission electron micrograph of grain boundary microcracking above the plane of the cyclic fatigue crack in AD 90 alumina. Fig. 9b is an example of intergranular microcracking in the same alumina specimen. Fig. 10a and b show distributed microcracking seen on the surface of an AD 90 alumina subjected to sustained load fracture at 1050°C. In addition to

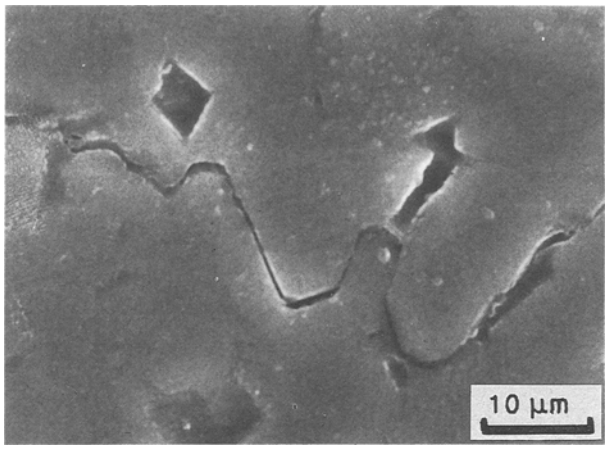

Figure 6 Microscopically tortuous crack path during static load fracture of AD 90 alumina at 1050°C. Note the absence of debris particles.

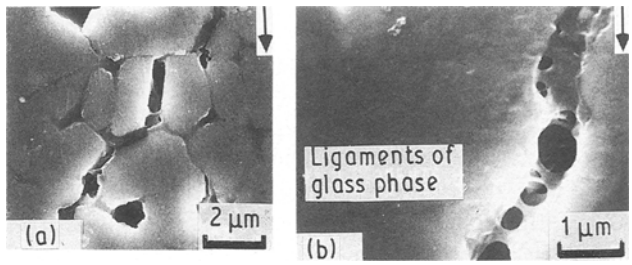

Figure 7 Static fracture characteristics of AD 90 alumina in 1050°C air. (a) Crack growth by intergranular fracture. (b) Ligaments of amorphous grain boundary films bridging the wake of the crack. The arrow indicates nominal direction of crack growth.

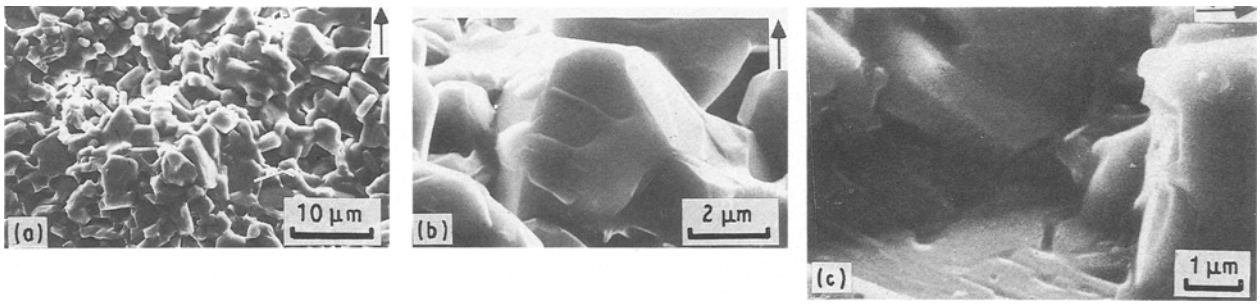

Figure 8 Scanning electron micrographs of cyclic fracture in AD 90 alumina in 1050°C air at $R = 0.15$ and $\nu_c = 0.13$ Hz. (a) Predominantly intergranular fracture mode. (b) Grain facets covered with amorphous films. (c) Sporadic occurrence of transgranular cleavage. Arrow indicates crack growth direction.

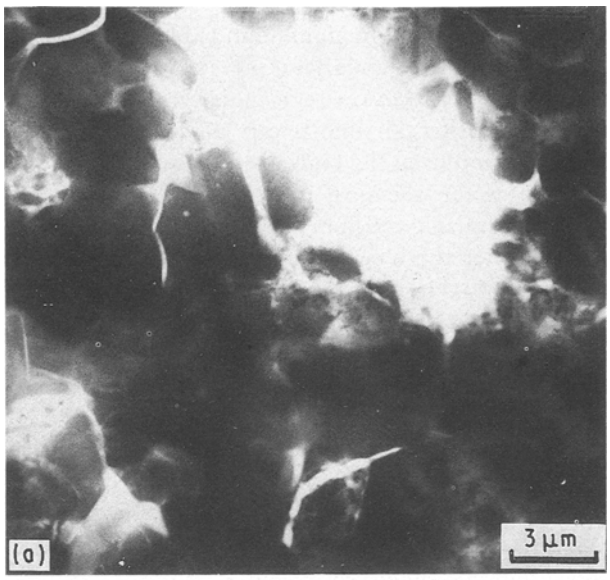

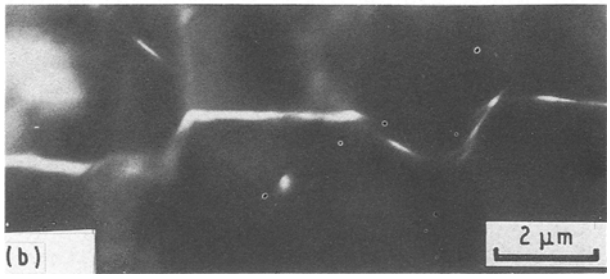

Figure 9 (a) Transmission electron micrograph of grain boundary microcracking above the plane of the (cyclic) fatigue crack (T = 1050°C, ν_c = 0.13 Hz, R = 0.15) in AD 90 alumina. The white region in the top centre is a hole created by ion milling. (b) Intergranular nature microcracking just above the plane of the main crack.

microcracking, the microscopically tortuous crack path and crack deflection can be seen in these micrographs.

From the above results it is readily seen that intergranular separation, aided by the presence of amorphous films along grain facets, plays a dominant role in influencing the subcritical growth of cracks in polycrystalline alumina in the high-temperature environment. The aforementioned results also point to some distinct differences in the contact along the crack faces, in the formation of debris particles within cracks, and in the manner in which amorphous films and debris particles are "squeezed out" of the cracks.

Finally, it is worth noting that in the AD 999 alumina with a significantly reduced glass phase content compared with AD 90 alumina, the fast crack growth under both static and cyclic loads (Fig. 4) produces a microscopic fracture morphology in which the absence of glass films on grain facets can be noticed (Fig. 11).

4. Discussion

The results of this work demonstrate that significant levels of subcritical crack growth occur in polycrystalline alumina under both static and cyclic loads. The

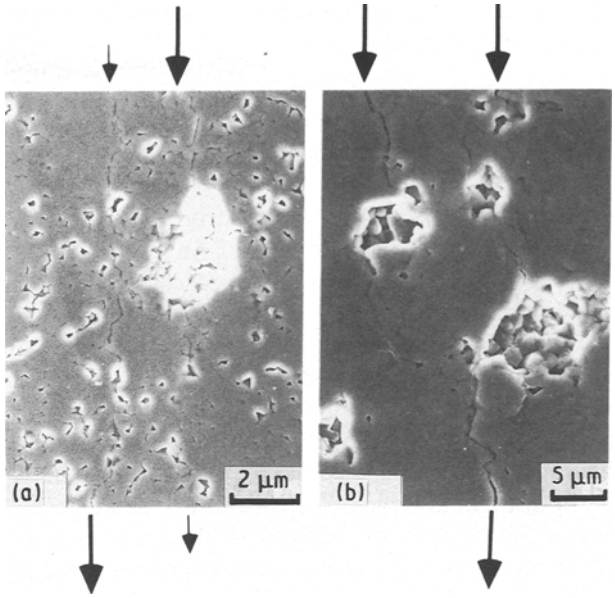

Figure 10 (a, b) Distributed microcracking and multiple cracking seen on the surface of AD 90 alumina subjected to static load fracture in 1050°C air. Crack growth directions for the main crack (larger arrows) and the secondary cracks (smaller arrows) are indicated.

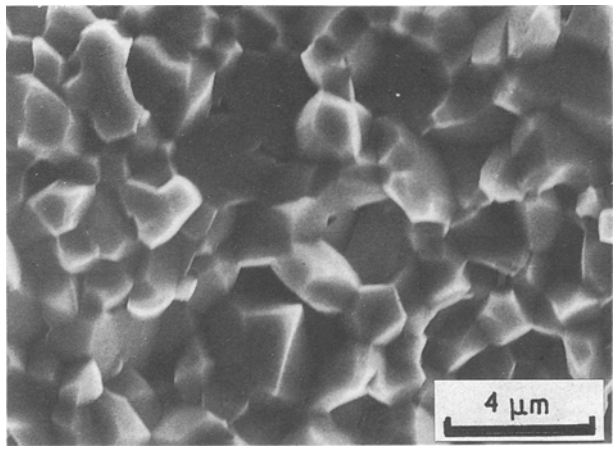

Figure 11 Scanning electron micrograph of the fracture surface of AD 999 alumina subjected to cyclic loading in 1050°C air at R = 0.15 and ν_c = 0.13 Hz.

primary mechanisms of static and cyclic fatigue fracture are similar in that they are both induced predominantly by intergranular separation. The presence of amorphous films, deposited along grain boundaries as a consequence of additives added during the processing of the ceramic, plays a decisive role in influencing the rates of fatigue crack growth. When the content of this amorphous phase is drastically reduced, as in the high-purity AD 999 alumina, the propensity for slow crack growth at low imposed values of stress intensity factors is also noticeably diminished.

4.1. Mechanisms

Despite the apparent similarities in the mechanisms of intergranular fracture, the static and cyclic fatigue

characteristics of polycrystalline alumina exhibit some important differences:

(i) The rates of fatigue crack growth under cyclic loading conditions are up to several orders of magnitude slower than those determined under sustained loads.

(ii) Cyclic crack velocities are strongly sensitive to the loading rate (i.e. test frequency). An increase in test frequency results in a decrease in crack velocities, as the crack is subjected to a smaller amount of time at the peak tensile stress. As the frequency is decreased or the maximum stress intensity factor is raised, the cyclic fatigue data begin to approach the static fatigue data.*

(iii) Static and cyclic crack growth behaviour are characterized by microscopically tortuous crack paths along grain boundaries, periodic branching and jumping of the crack front, bridging of the crack faces by ligaments of the viscous amorphous film, and bridging of the crack faces by grain facets. However, under cyclic loading conditions, further alterations to the fracture process appear to occur as a result of (a) the formation of debris particles due to repeated contact between the crack faces, (b) fretting and enhanced roughness-induced crack closure arising from locally mixed-mode opening and closing (e.g. [29]), (c) "squeezing out" of the debris particles and amorphous films from within the crack by the pumping action of the crack walls, and (d) sensitivity of the deformation and flow of the amorphous film to the loading rate.

The results of our work also indicate that caution should be exercised in attempting to derive cyclic crack growth rates solely on the basis of static fatigue data. The cyclic fatigue data may approach the static fatigue data at extremely slow loading rates (low cyclic frequencies, typically smaller than 0.01 Hz) or for long hold times at the peak stress of the fatigue cycle. However, at higher frequencies or at lower hold times, our results show that simple correlations between static and cyclic fracture do not hold (see the results of Fig. 3).

It is interesting to note that the results of this study are also consistent with recent work on the high-temperature crack growth behaviour of Al_2O_3, Si_3N_4 and Al_2O_3–SiC composite under cyclic loads [24, 27–29]. In all these studies, cyclic loading is found to provide a more beneficial response than static loading at high temperature. This trend is at variance with the behaviour seen at room temperature in both monolithic ceramics and transformation-toughened ceramics where cyclic loading has a more deleterious effect on resistance to fracture than static loading [22, 30]. This difference can be attributed to the combined effects of creep, deformation of the viscous phase and the aforementioned processes of crack-wake contact.

4.2. Role of glass phase

In the present tests on aluminium oxide, the amorphous film at grain boundaries is a pre-existing phase left from processing. However, in some ceramics and ceramic composites, an amorphous glass phase can also form *in situ* during the high-temperature fracture test because of the chemical interaction of the material with an oxidizing medium such as air. An example of such a material is a ceramic composite made up of an aluminium oxide matrix with a reinforcement of silicon carbide whiskers. A comparison of the present results on polycrystalline Al_2O_3 with similar results obtained by Han and Suresh [24] for an Al_2O_3–33 vol% SiC whisker composite provides interesting information on the role of glass phase in influencing static and cyclic fatigue behaviour. (The results obtained by Han and Suresh [24] involved flexural test specimens, pre-cracking methods and loading conditions that are identical to those employed in the present study.)

SiC whiskers in the Al_2O_3–SiC composite oxidize when exposed to air at temperatures typically in excess of 1250°C. A product of this reaction is SiO_2 glass phase which penetrates the interface between SiC and Al_2O_3.‡ As the glass phase becomes viscous in the high-temperature environment, stress-assisted viscous flow of the molten glass results in extensive cavitation along the Al_2O_3–SiC interfaces and at grain triple junctions in the regions ahead of the crack tip. Creep deformation arising from the formation of interfacial cavities is more pronounced when the viscosity of the glass is low and when the glass phase wets or penetrates the grain facets [32–34].

In an unnotched or uncracked specimen of the Al_2O_3–SiC composite, the oxidation of SiC is confined to near-surface regions because the oxygen in air does not penetrate through the bulk of the material to the interior sections by random-walk diffusion during the test. However, in a notched and/or pre-cracked specimen with a through-thickness crack, the transport of the oxidizing species to the highly stressed region of the crack tip promotes oxidation of SiC and cavitation due to the viscous flow of glass, uniformly through the thickness of the specimen. The nucleation, growth and coalescence of cavities results in the formation of a diffuse microcrack zone ahead of the main crack-tip.

Fig. 12a is a transmission electron micrograph of a SiC whisker located in the crack-tip region in the Al_2O_3–SiC composite which was subjected to sustained load fracture in 1400°C air. Prolonged exposure of the SiC to the high-temperature oxidizing environment under the influence of a sustained peak stress ($K_I \approx 3.5$ MPa $m^{1/2}$) results in the conversion of a significant fraction of the whisker to glass pockets (the white regions denoted by arrows). However, if the

*Although the present study has focused on only one cyclic waveform (i.e. sinusoidal), it is to be expected that the waveform and the hold time at the peak stress will have a marked effect on crack growth behaviour at elevated temperatures. Recent work [27] on stress–life response in alumina at 1200°C reveals that cyclic loading with a short duration of maximum stress provides a beneficial effect on fatigue lifetime as compared to static loading with the same maximum stress. Increasing the hold time at the maximum stress brings the fatigue life closer to the static lifetime under comparable values of maximum applied stress.

‡Full details of this reaction between SiC, Al_2O_3 and O_2 in air are not known at the present time. However, the matrix Al_2O_3 can also react with silica glass to form aluminosilicate glasses and SiC-rich or stoichiometric mullites, if given sufficient time [31]. For the conditions of the experiments quoted here [24], the principal product of oxidation of SiC is SiO_2 glass.

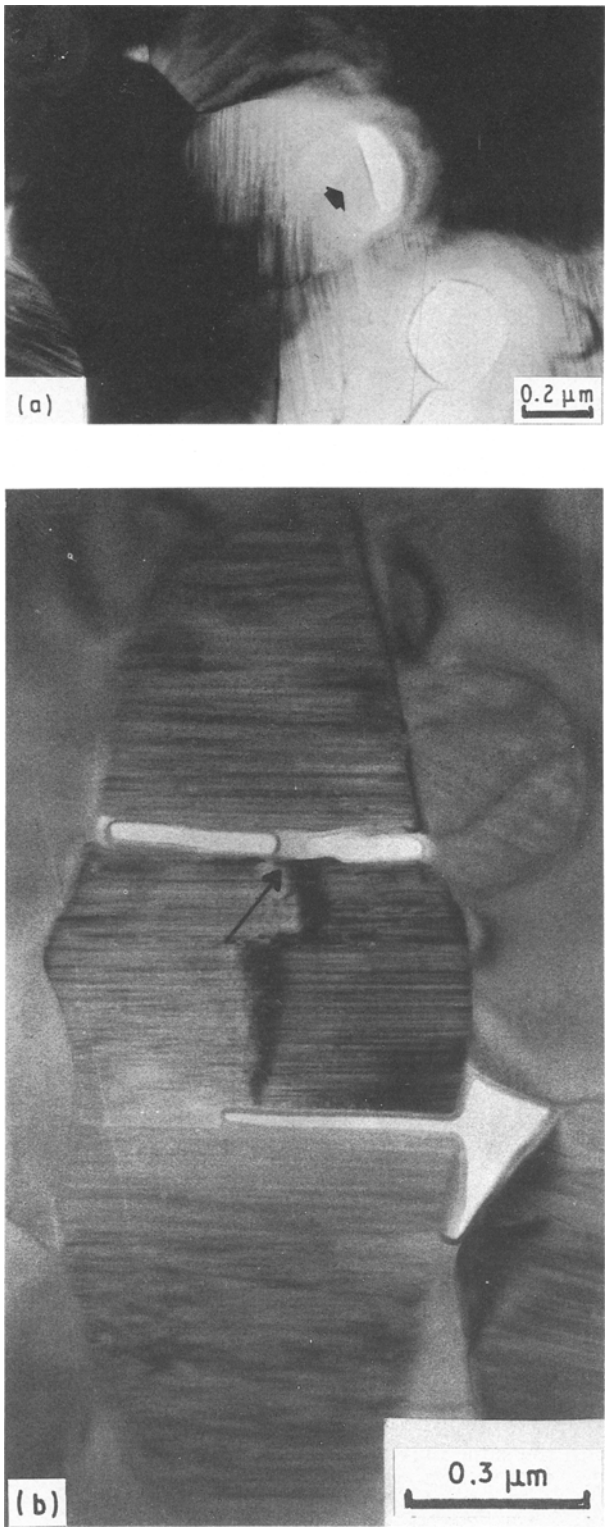

Figure 12 Transmission electron microscopy of crack-tip damage in Al_2O_3–33 vol% SiC whisker composite in 1400°C air [24]. (a) Conversion of a significant fraction of the fracture surface (white regions) into glass pockets under sustained loads ($K_I \sim 3.5$ MPa $m^{1/2}$). (b) A whisker broken by cyclic loading ($R = 0.15$ and $\nu_c = 0.1$ Hz). Note the meniscus of glass within the broken whisker (denoted by the arrow).

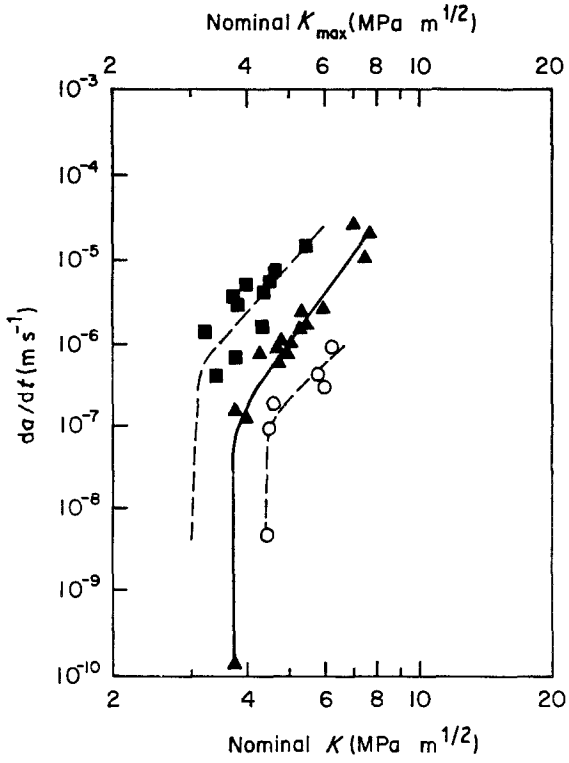

Figure 13 (■) Crack velocity plotted against the stress intensity factor for Al_2O_3–SiC whisker composite subjected to static fracture in 1400°C air [24]. Also shown are experimentally measured crack velocities, $da/dt = \nu_c(da/dN)$, as a function of $K_{max} = \Delta K/(1 - R)$ for cyclic load fracture in 1400°C air at $R = 0.15$ and ν_c = (▲) 0.1 Hz and (○) 2 Hz.

ceramic composite is subjected to cyclic loads (even with the maximum stress intensity factor in the cyclic test being the same as that in the static load tests), such extensive oxidation of a single whisker of SiC is not observed because of periodic unloading. On the other hand, cyclic loading causes the SiC whiskers in the crack-tip region to break. Fig. 12b is a transmission electron micrograph showing a broken whisker from a cyclic fatigue test ($K_{max} = 3.5$ MPa $m^{1/2}$, $R = 0.15$, $\nu_c = 0.1$ Hz, 1400°C air). Note the meniscus of the molten glass phase (indicated by the arrow) flowing inside the broken whisker.

The variation of crack velocity, da/dt, in the Al_2O_3–SiC composite is plotted in Fig. 13 as a function of the applied stress intensity factor K_I for the static crack growth experiments conducted in air. Also shown in this figure are the crack velocities, $da/dt = (da/dN)\,\nu_c$, as a function of the maximum stress intensity factor, K_{max}, for the cyclic fatigue tests conducted on the ceramic composite at 1400°C at $R = 0.15$, and $\nu_c = 0.1$ and 2 Hz. As in the trend seen for the alumina ceramic (Fig. 3), cyclic crack growth in the ceramic composite is significantly lower than that seen under static loads. Furthermore, an increase in test frequency results in a reduction in the rates of fatigue crack growth. It is also found that the cyclic crack growth rates, predicted on the basis of static crack growth rates (similar to the procedure used in connection with Fig. 3), deviate markedly from experimental results.

4.3. On mechanical fatigue effects in ceramics

The present work illustrates that, despite the similarities in many failure mechanisms between static and cyclic fatigue in alumina, some mechanical fatigue effects also occur in the elevated-temperature environment. On the basis of information available in the

literature (e.g. [20, 21, 29]) and of the results of the present work, the occurrence of cyclic fatigue effects in brittle solids can be identified using the following definitions:

(i) A mechanical (cyclic) fatigue effect in which the macroscopic mode of fracture under cyclic loads is distinctly different from that seen under monotonic loads.

(ii) A microscopic fatigue effect in which the mechanism of deformation under cyclic loads is distinctly different from that seen under static loads.

(iii) A micromechanical fatigue effect wherein kinematically irreversible cyclic deformation arises in ceramic materials as a consequence of microcracking, phase transformations, creep, interfacial sliding or crack bridging, analogous to slip irreversibility in metal fatigue.

(iv) A mechanical fatigue phenomenon arising from crack-wake effects wherein differences in crack closure, glass-phase deformation, crack bridging or grain bridging result in apparently different crack growth rates between static and cyclic fatigue, even though the basic micromechanisms of deformation and failure are similar.

The results discussed in this paper provide supporting evidence for the existence of a mechanical fatigue effect on the basis of the last two definitions given above.

4.4. Further considerations

This work has identified several key mechanisms of elevated-temperature crack growth in polycrystalline alumina subject to static and cyclic loads. However, a more detailed understanding of this subject inevitably calls for further work where the effects of test temperature, load ratio, test frequency, cyclic waveform and hold time on crack propagation rates are examined. In addition, the effects of environment on crack growth, particularly on the deformation of the glass phase, need to be addressed in greater detail. The humidity of the air environment is expected to have a detrimental effect on the strength of the glassy phase. Water in the air will react with the glass, especially at crack-tip locations where the glass is highly stressed. The ensuing chemical reaction can be written as [35]

$$H_2O\,(\text{atmosphere}) \rightleftharpoons H_2O\,(\text{in glass}) \quad (2)$$

$$H_2O\,(\text{in glass}) + [\text{Si–O–Si}] \rightleftharpoons 2[\text{SiOH}] \quad (3)$$

This reaction leads to a break in the Si–O bond in the glass. The attendant reaction with the water molecule proceeds according to Equation 3.

The experimental results on AD 90 and AD 999 alumina as well as those on the Al_2O_3–SiC composite also point to appealing possibilities for the design of ceramic materials with improved resistance to elevated-temperature crack growth. If the presence of amorphous films along grain boundaries and interfaces has a significant effect on crack growth, judicious manipulations of the chemistry, volume fraction and distribution of such phases can provide enhanced resistance to subcritical fracture. These issues should form topics of future research.

5. Conclusions

1. The application of static and cyclic loads to precracked four-point bend specimens of a 90% pure polycrystalline alumina causes subcritical crack growth over the (maximum) stress intensity factor range 1.5–5 MPa $m^{1/2}$ in 1050°C air.

2. The rates of crack growth under cyclic loading conditions are up to two orders of magnitude slower than those found under static loading (of the same magnitude as the maximum stress intensity factor from cyclic load). Cyclic crack velocities are markedly influenced by the loading frequency, with an increase in test frequency reducing the crack growth rate.

3. Crack growth under static and cyclic loads occurs predominantly by an intergranular fracture process, with the presence of the grain-boundary glass phase playing an important role in the microscopic separation of grain facets.

4. Apparent differences between static and cyclic crack growth results can be, at least partially, attributed to the following effects of cyclic loads: (i) the formation of debris particles due to the repeated contact between the mating fracture surfaces, (ii) contact of fracture surface asperities and enhanced roughness-induced crack closure due to locally mixed-mode opening and closing of the crack, (iii) pumping action of the crack walls which squeeze out the debris particles and the viscous glass films from the crack, and (iv) rate-sensitivity of deformation in the glass phase. Our results show that cyclic crack growth rates cannot be predicted solely on the basis of static fracture data.

5. Subcritical crack growth at high temperatures in a fine-grained alumina of high purity (AD 999) is significantly less pronounced than in the 90% pure alumina. This result implies that a certain minimum amount of glass phase may be necessary to induce marked levels of stable crack growth.

6. Both the static and cyclic fatigue crack growth characteristics in 90% pure alumina are qualitatively similar to those reported earlier for an Al_2O_3–SiC whisker composite in the elevated-temperature environment. The present results are also consistent with the conclusions of recent studies of high-temperature fatigue life in alumina at 1200°C, where cyclic loading results in a longer time to failure than static loading with the same maximum tensile stress.

Acknowledgement

This work was supported by the Basic Science Division of US Department of Energy under Grant DE-FG02-84ER-45167 to Brown University.

References

1. A. G. EVANS and E. R. FULLER, *Metall. Trans.* **5A** (1974) 27.
2. S. LATHABAI, Y.-W. MAI and B. R. LAWN, *J. Amer. Ceram. Soc.* **72** (1989) 1760.
3. T. KAWAKUBO, N. OKABE and T. MORI, in "Fatigue 90", Vol. 2, edited by H. Kitagawa and T. Tanaka (Materials and Component Engineering Publications Ltd, Birmingham, 1990) p. 717.
4. J. S. MIZUSHIMA and W. J. KNAPP, *Ceram. News* **5** (1956) 26–29, 36.

5. H. N. KO, *J. Mater. Sci. Lett.* **5** (1986) 464.
6. *Idem, ibid.* **8** (1989) 1438.
7. K. C. LIU and C. R. BRINKMAN, in Proceedings of 24th Automotive Technology Development Contractors' Meeting, P-197 (Society of Automotive Engineers, Warrendale, PA, 1987) p. 191.
8. L. S. WILLIAMS, *Trans. Br. Ceram. Soc.* **55** (1956) 287.
9. C. P. CHEN and W. J. KNAPP, in "Fracture Mechanics of Ceramics", Vol. 2, edited by R. C. Bradt, D. P. H. Hasselman and F. F. Lange (Plenum, New York, 1974) p. 691.
10. D. A. KROHN and D. P. H. HASSELMAN, *J. Amer. Ceram. Soc.* **55** (1972) 208.
11. A. G. EVANS, *Int. J. Fract.* **16** (1980) 485.
12. E. B. SHAND, *Amer. Ceram. Soc. Bull.* **38** (1959) 653.
13. R. SEDLACEK and F. A. HALDEN, in "Structural Ceramics and Testing of Brittle Materials", edited by S. J. Acquaviva and S. A. Bortz (Gordon & Breach, New York, 1968) p. 211.
14. B. K. SARKAR and T. G. J. QUINN, *Trans. Br. Ceram. Soc.* **69** (1970) 199.
15. F. GUIU, *J. Mater. Sci. Lett.* **13** (1978) 1357.
16. L. EWART and S. SURESH, *ibid.* **5** (1986) 774.
17. *Idem, J. Mater. Sci.* **22** (1987) 1173.
18. J. R. BROCKENBROUGH and S. SURESH, *J. Mech. Phys. Solids* **35** (1987) 721.
19. S. SURESH and J. R. BROCKENBROUGH, *Acta Metall.* **36** (1988) 1455.
20. S. SURESH, in "Fatigue 90", Vol. 2, edited by H. Kitagawa and T. Tanaka (Materials and Component Engineering Publications Ltd, Birmingham, 1990) p. 759.
21. *Idem, Int. J. Fract.* **42** (1990) 41.
22. M. J. REECE, F. GUIU and M. F. R. SAMMUR, *J. Amer. Ceram. Soc.* **72** (1989) 348.
23. A. G. EVANS, L. R. RUSSELL and D. W. RICHERSON, *Metall. Trans.* **6A** (1975) 707.
24. L. X. HAN and S. SURESH, *J. Amer. Ceram. Soc.* **72** (1989) 1233.
25. L. X. HAN, R. WARREN and S. SURESH, *Acta Metall. Mater.* **40** (1992) 259.
26. L. EWART, PhD thesis, Brown University (1990).
27. C.-K. J. LIN and D. F. SOCIE, *J. Amer. Ceram. Soc.* **74** (1991) 1511.
28. T. FETT, G. HIMSOLT and D. MUNZ, *Adv. Ceram. Mater.* **1** (1986) 179.
29. S. SURESH, "Fatigue of Materials" (Cambridge University Press, Cambridge, England, 1991) pp. 403–56.
30. R. H. DAUSKARDT, D. B. MARSHALL and R. O. RITCHIE, *J. Amer. Ceram. Soc.* **73** (1990) 893.
31. P. F. BECHER and T. N. TIEGS, *Adv. Ceram. Mater.* **3** (1988) 148.
32. R. RAJ, *J. Amer. Ceram. Soc.* **69** (1986) 708.
33. K. JAKUS, S. M. WIEDERHORN and B. J. HOCKEY, *ibid.* 725.
34. J. R. PORTER, *Mater. Sci. Engng* **A107** (1989) 127.
35. S. W. FREIMAN, in "Strength of Inorganic Glass", edited by C. R. Kurkjian (Plenum, New York, 1985) p. 197.

Received 29 May
and accepted 2 October 1991